RESEARCH ARTICLE

Characterization of transonic shock oscillations over the span of an OAT15A profile

Alessandro Accorinti[1] · Tim Korthäuer[1] · Sven Scharnowski[1] · Christian J. Kähler[1]

Abstract

The flow over a wing model with aspect ratio 2 and based on the supercritical airfoil (OAT15A) was experimentally investigated for a fixed Reynolds number (Re_c) of 3×10^6 and numerous aerodynamic conditions. The angle of attack (AOA) and the Mach number (M_∞) were varied between 5° and 6.5°, and between 0.72 and 0.75, respectively. Here we focused on the dynamics of the shock front at incipient and developed buffet conditions, by employing background-oriented schlieren measurements on the wing's upper surface. The spanwise variations of the shock front statistics and its frequency content were examined. The shock oscillations appeared to be the superposition of multiple fluid modes, of which the most dominant was the classic 2-D buffet, which induced uniform chordwise oscillations of the shock front. The hypothesis was formulated that the remaining modes are linked to physical phenomena reported in the literature, namely the side-wall boundary layer and the vortices detected in the mid-span separated flow.

List of symbols

σ	Standard deviation
ζ	Normal distance to the upper surface (mm)
c	Chord (mm)
f	Frequency (Hz)
h_t	Height of the tripping dots (μm)
k	Reduced frequency; $\pi f c / U_\infty$
M_∞	Free-stream Mach number
p_0	Stagnation pressure (Pa)
Re_c	Reynolds number based on the chord
Re_{h_t}	Reynolds number based on the height of the tripping dots
s	Span (mm)
St	Strouhal number; $f c / U_\infty$
T_0	Stagnation temperature (K)
U_∞	Free-stream velocity upstream of the model (m/s)
x	Streamwise distance from the leading edge (mm)
x_s	Shock position (mm)
y	Spanwise distance from the centerline (mm)
z	Vertical distance from the leading edge (mm)

1 Introduction

Self-sustained shock oscillations, namely shock buffet, may take place on the upper surface of a wing under several combinations of transonic Mach number (M_∞) and angle of attack (AOA). In the case of a completely rigid wing, this phenomenon induces unsteady aerodynamic loads, which may shorten the fatigue life of the aircraft. If the wing is flexible, a fluid-structure interaction (FSI) can occur, which is defined as buffeting. This is facilitated by the fact that buffet frequency is usually on the same order of magnitude as low structural (for instance pitching or heave) eigenfrequencies. If the structural oscillations grow in amplitude and become remarkably large, the structural integrity of the wing itself can be endangered. For this reason, buffet, along with other aeroelastic phenomena (for instance, the classic one-degree-of-freedom flutter), limits the flight envelope of civil aircraft and their cruise speed.

Even though the physical working principle of buffet is yet to be thoroughly unveiled, the effort that the scientific

✉ Alessandro Accorinti
alessandro.accorinti@unibw.de

1 Institute of Fluid Mechanics and Aerodynamics, Bundeswehr University Munich, Werner-Heisenberg-Weg 39, Neubiberg 85577, Germany

community has put in the last century contributed to gathering a common understanding of it.

1.1 Flow development from steady shock to buffet

The key steps of the flow development from steady shock to shock buffet were identified and can be summarized by the following series of subsequent aerodynamic states: steady shock (normal shock motion), separation of the boundary layer, inversion of the shock motion, buffet onset, developed buffet, and buffet offset. At low Mach numbers and angles of attack, the shock is steady. A small increase in one of these aerodynamic parameters would slightly shift the shock toward the trailing edge. Such a response is called normal shock motion and can be thought of as an adjustment of the pressure distribution on the model to satisfy the equality and compatibility conditions of the pressure at the trailing edge (Pearcey 1958).

If the Mach number and/or the angle of attack are significantly increased, a separation of the boundary layer may ensue either at the shock foot or at the trailing edge, depending on the wing geometry (Crouch et al 2009a; Iovnovich and Raveh 2012). In general, the separation of the boundary layer was found to be a necessary condition for the occurrence of buffet (McDevitt and Okuno 1985; Nitzsche 2009; Deck 2005; Thiery and Coustols 2005; Iovnovich and Raveh 2012; Jacquin et al 2009; Crouch et al 2009b; Lee 1990; Giannelis et al 2018; Sartor et al 2015; Brion et al 2017; Nitzsche et al 2019; D'Aguanno et al 2021; Accorinti et al 2022).

By progressively raising the Mach number and/or the angle of attack, the extent of the separated region grows, until the shock begins to travel upstream with an increase in AOA or M_∞. This phenomenon is called inversion of the shock motion and allows for satisfying the equality and compatibility conditions once the separation considerably affects the pressure distribution on the model. Already presented in Pearcey (1958) as a sign of separation of the boundary layer, it was recently proved in Accorinti et al (2022) to be a necessary condition for buffet onset in the case of constant Mach number and AOA sweep.

Buffet onset is commonly defined as the aerodynamic condition at which the fluctuations of one quantity in the flow (for instance the pressure on the upper surface in Jacquin et al (2009), or the lift coefficient in Iovnovich and Raveh (2012) and Giannelis et al (2018), or the shock location in Accorinti et al (2022) and Korthäuer et al (2022)) exceeds an arbitrary threshold. As of the onset, the shock starts to oscillate in the streamwise direction. However, as shown in Jacquin et al (2009) and Accorinti et al (2022), a further increase in AOA or M_∞ is needed to establish developed periodic shock oscillations at a dominant frequency ($0.16 < k < 0.22$ and $0.05 < St < 0.07$ are typical

ranges of buffet reduced frequency and Strouhal number, respectively).

The amplitude of the shock oscillations soars with an additional increase in angle of attack and/or Mach number, up to reaching a maximum. Then, it diminishes, until buffet is extinguished, and the shock appears steady again. This condition is called buffet offset, and delimits, together with buffet onset, the range of aerodynamic parameters where shock oscillations can be observed.

1.2 Physical interpretations and theoretical models

Two main theoretical models of shock buffet have been proposed over the last decades, which attempt to give a physical interpretation to this phenomenon.

According to the model presented in Lee (2001), shock buffet is sustained by a feedback mechanism between downstream and upstream traveling waves (UTWs). The downstream traveling waves (DTWs) are originated at the shock foot and travel within the boundary layer toward the trailing edge. There, as a consequence of their passage, acoustic waves are generated in the outer flow, which head toward the shock, reach it, and complete the feedback. Based on this assumption, the buffet frequency was computed as the inverse of the sum of the characteristic times of the downstream and upstream traveling waves. The so estimated buffet frequency agreed fairly well with the one measured by the force balance. Following the work of Lee (2001), other research groups (Xiao et al 2006; Deck 2005; Jacquin et al 2009; Garnier and Deck 2010; Hartmann et al 2013) used Lee's model to compute the buffet frequency, leading to contradictory results. In fact, in Xiao et al (2006), Deck (2005) and Hartmann et al (2013), the so estimated buffet frequency agreed well with the one directly measured in the flow. However, in Jacquin et al (2009) and Garnier and Deck (2010), Lee's model led to highly inaccurate values of buffet frequency. The main issue is that the propagation properties, especially the convective velocity of the downstream traveling structures, are extremely sensitive to the assumptions and simplifications made (see Kokmanian et al (2022) for more details).

A second interpretation of the buffet phenomenon, which is based on an unstable shock-wave/separation bubble interaction, was given by Raghunathan et al (1998). In this work, it was shown that the formation of a large enough separation bubble plays a key role in the onset of shock oscillations. The effective geometry (camber) is modified by the presence of the bubble, and the shock has to move on the upper surface of the wing according to the extent of the separated region. In particular, the expansion and collapse of the separation bubble are responsible, respectively, for the upstream and downstream displacement of the shock during a buffet cycle. This dynamic adjustment of the shock location

is similar to the static one reported for an increase in AOA in Pearcey ([1958](#)), even though in that case the highlighted triggering factor was not the change in effective geometry, but the drop of pressure values in the vicinity of the trailing edge.

More of a practical approach, which provides a highly reliable estimation of the buffet onset and frequency, is the so-called global modal decomposition of the transonic equations of the flow. This method was first applied in Crouch et al ([2009b](#)) to compute the aerodynamic modes of the flow, and to identify the one that becomes unsteady with an increase in AOA. The flow field associated with this unsteady mode is characterized by a coupled shock oscillation and pulsation of the separated boundary layer. The buffet onset and frequency were estimated this way for different Mach numbers, AOA, and geometries, yielding a good agreement with the experimental results of McDevitt and Okuno ([1985](#)) and Jacquin et al ([2009](#)). Also in Sartor et al ([2015](#)), a global stability analysis was performed, which compares favorably with the results in Jacquin et al ([2009](#)) and Crouch et al ([2009b](#)).

1.3 Spanwise variation of shock front features on 2-D wings

In Jacquin et al ([2009](#)), a wing with an OAT15A profile and aspect ratio of 3.4 was examined. Oil flow visualizations were employed to highlight some of the flow features at two different angles of attack and one Mach number. For the pre-buffet condition, the time-averaged shock front appeared straight for most of the span. Moreover, a uniform shock-induced separation bubble was visible. However, in the last 10% of the span at each wing end, the shock location curved upstream and the flow behind the shock remained attached. This latter phenomenon was traced back to the interaction with the side-wall boundary layer.

At a higher angle of attack, buffet took place. No remarkable changes could be noted in terms of time-averaged shock front. However, steady vortices were detected in the shock-induced separated area in the middle of the span, which were also found in the numerical simulation of Thiery and Coustols ([2005](#)) for the same model and combination of aerodynamic parameters. Even though this 3-D feature appeared, the frequency content of the pressure sensors, which were all at a fixed chordwise position and covered 10% of the span in the central section of the wing, displayed a clear and dominant contribution only at the buffet frequency. These apparently contradictory results were explained in Jacquin et al ([2009](#)), by stressing that pressure taps and oil-film flows characterize different quantities: the pressure is regulated by the Euler flow above the viscous layers and is of order U_∞^2, whereas the oil-film captures the wall velocity field, which

is an order of magnitude lower than U_∞. This suggests that the velocity associated with the 3-D vortices in the mid-span region is small compared to the longitudinal velocity above the detached flow, and, therefore, does not appreciably contribute to the pressure fluctuations measured by the taps.

The authors advanced three possible physical interpretations of the co-presence of 2-D and 3-D buffet aspects on the investigated 2-D wing. The first one contemplates the superposition of a strong 2-D global mode with a weaker 3-D one. According to the second interpretation, a transition from a 2-D to a 3-D mode could take place, once buffet onset occurs. The third and last conjecture traces back the development of 3-D features in the mid-span portion to the influence exerted on the flow by the side-wall boundary layer.

In D'Aguanno et al ([2021](#)), a wing with an OAT15A profile and an aspect ratio of 2 was investigated. The phase-averaged velocity field obtained via particle image velocimetry (PIV) revealed a rather straight shock front in the central part of the span ($-0.125 \le y/s \le 0.125$). This was valid for both the upstream and downstream shock locations of the buffet cycle. The UTWs too exhibited a near-zero average inclination in the central part of the span. However, the power density function of the UTW inclination showed that the instantaneous inclination can significantly deviate from the zero value. Moreover, the instantaneous shock front captured via PIV and BOS showed a non-negligible curvature.

In Sugioka et al ([2022](#)), similar results to Jacquin et al ([2009](#)) were found. Instantaneous oil flow visualizations were used to study the evolution of flow from pre-buffet to buffet conditions over a 2-D wing, based on the NASA CRM airfoil and with an aspect ratio of 4.5. At pre-buffet conditions, two different flow topologies were detected along the span. For most of the span, the shock front was straight and induced a uniform separation bubble. However, in the last 15% of the span at each wing end, the flow remained attached due to the interaction with the side-wall boundary layer. At a higher angle of attack, the shock started to oscillate. Moreover, a new topology characterized by trailing edge separation emerged in the proximity to the mid-span section. There, vortical structures possibly linked to those reported in Jacquin et al ([2009](#)) were visible. Further increasing the angle of attack led to an expansion of the trailing edge separation toward the span ends. Furthermore, the effects of the side-wall boundary layer seemed to be confined to less than 10% of the span at each wing end.

1.4 Structure and goals of the paper

In Jacquin et al ([2009](#)) and Sugioka et al ([2022](#)), oil flow visualizations and pressure measurements gave important insights into the spanwise variation of the shock front on a nominally 2-D wing. However, a description of the shock

dynamics is missing. The aim of the present work consists in providing the time-resolved spanwise shock front locations for several combinations of aerodynamic parameters (angle of attack and Mach number). Specifically, the following goals can be defined:

- Determine the statistics (time average and standard deviation) of the entire shock front. In particular, investigate the influence of the side-wall boundary layer on the curvature and on the oscillation amplitude of the shock front.
- Determine the frequency content of the shock front for buffet flows. In particular, verify whether it is constant across the entire span and whether it exhibits other contributions than the expected 2-D buffet frequency.
- Establish whether the shock uniformly oscillates across the span or a phase lag in the shock oscillations appears, moving from the mid-span region to the wing ends. The latter is a typical feature of 3-D buffet (Iovnovich and Raveh 2015). Even though the model in the present work does not have any sweep angle, it cannot be excluded that the presence of the 3-D features reported in Jacquin et al (2009) and Sugioka et al (2022) introduces a phase lag between shock oscillations at different spanwise positions.

The rest of the paper is structured as follows. In Sect. 2, the experimental setup is presented. The facility as well as the model and the measurement technique are described. In Sect. 3, the statistics, the frequency content, and the correlation of the shock front determined via background-oriented schlieren (BOS) are presented. Finally, some concluding remarks are outlined in Sect. 4.

2 Experimental setup

2.1 Trisonic wind tunnel Munich

The Trisonic wind tunnel Munich (TWM) facility is a blow-down wind tunnel with a 300 mm wide and 680 mm high test section ideally suited for profile measurements. The facility has a M_∞ operating range from 0.2 to 3.0. The Reynolds number can be adjusted by means of the total pressure, which can be varied between 1.2 and 5.0 bar. The facility has two tanks with a total volume of 356 m^3 that are pressurized with dry air up to 20 bar above ambient pressure. This allows for a maximal run time of 100 s for the flow conditions in this work. The free-stream turbulence level based on the streamwise velocity fluctuations in the TWM test section is 1.9% at $M_\infty = 0.3$ and decreases with increasing M_∞, reaching 0.45% at $M_\infty = 3.0$, as shown in Scharnowski et al

(2019). More details about the facility and its characterization are provided in Scheitle and Wagner (1991).

In order to compensate for the growth of the boundary layer in the test section, a boundary layer suction is applied to the side walls, and the test section height is increased moving downstream. In the range of aerodynamic parameters investigated in the present work, the thickness of the side-wall boundary layer is approximately 20 mm.

The blockage effects introduced by the model are deemed to have a minor impact since the blockage ratio is below 3.5% at the highest AOA considered in this work. However, as reported in Accorinti et al (2022), the suction may excessively reduce the local Mach number on the wing in the presence of shock waves and contribute to the delay in buffet development with respect to the literature.

2.2 OAT15A model

The model under investigation is based on the OAT15A profile, developed by ONERA.

The carbon-fiber-reinforced polymer (CFRP) airfoil has a relative thickness of 12.3%, a chord length $c = 152$ mm, a span $s = 298$ mm ($AR = 2$) and a trailing edge thickness of 0.5% of the chord. Between the model and the side windows of the test section, there is a gap of 1mm, whose effect on buffet was presented in Accorinti et al (2022). The boundary layer is tripped at the position $x/c = 0.07$ by applying on both the upper and lower surface a row of circular dots with a diameter of 3 mm, 70 μm high, and distributed every 6 mm along the span. The successful boundary layer tripping at the desired location is confirmed by inspection of the BOS raw data. The dot height, h_t, is selected to trigger the transition to turbulence without overtripping. In particular, h_t satisfies the relevant condition indicated in Thiery and Coustols (2005): $Re_{h_t} = \frac{Re_c h_t}{c} > 900$.

The profile is rigidly mounted in the wind tunnel to impede FSI. However, hammer tests performed on the model in absence of flow revealed that the first three Eigen frequencies – heave, pitch coupled with surge, and pitch - are relatively low (158, 300, and 389 Hz, respectively) and close to the expected buffet frequency. Deformation measurements were employed in Accorinti et al (2022) to assess the actual rigidity of the model and its interaction with the flow. The results showed that the model can be considered rigid regarding pitch motion. However, the same cannot be said for the heave motion, for which the oscillations increase by one order of magnitude with buffet onset. More information about the deformation measurements can be found in Accorinti et al (2022).
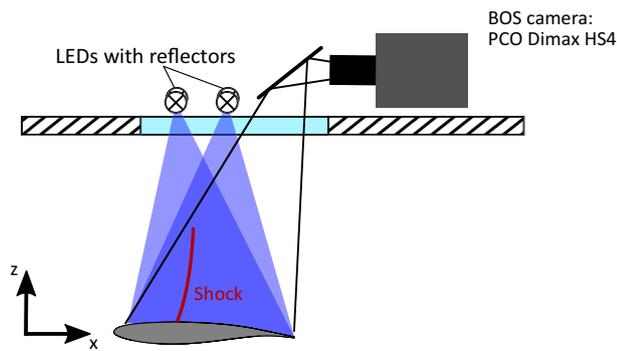
Fig. 1 Side view of the experimental setup
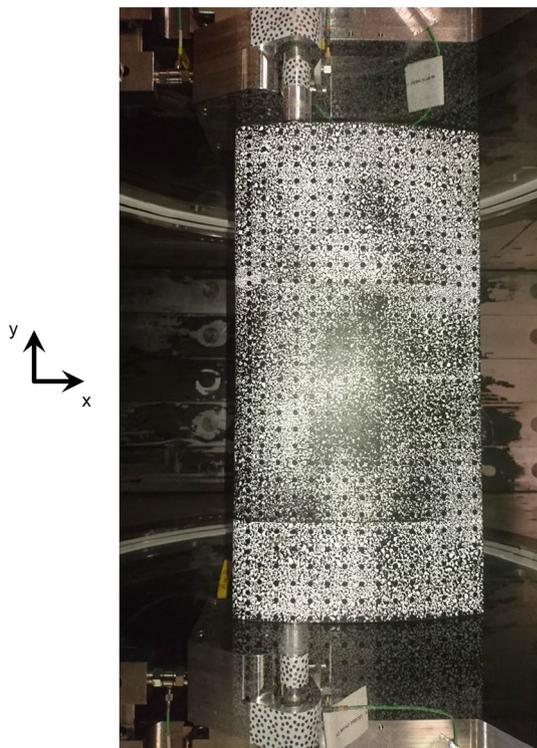
Fig. 2 Top view of the model with the applied speckle pattern

2.3 Background-oriented Schlieren

In Fig. 1, the side view of the test section and of the experimental setup is illustrated. In order to perform BOS measurements from the top of the test section, a random speckle pattern, approximately 50 μm high, is painted with a sponge on the model's upper surface, as can be seen in Fig. 2. The regular point-like pattern visible in the same picture was used, as first attempt, for the digital image correlation measurements reported in Accorinti et al (2022). The height of both the dot and the speckle patterns projects out of the

purely viscous sublayer ($\approx 10\mu$m). The state of the model's surface belongs to what Schlichting and Gersten (2017) defines as "transition region" from "hydraulically smooth" to "fully rough". Therefore, roughness effects cannot be considered completely negligible. The light coming from two LEDs (Luminus CBM-120-UVX, 405nm) on top of the test section is scattered by the model and reaches a PCO Dimax HS4 camera mounted on top of the test section. The displacement of the background pattern between wind-off and wind-on (without and with the flow in the test section) is proportional to the density gradient at wind-on conditions. The displacement field is evaluated by performing a cross-correlation between the two images and provides a qualitative representation of the density gradient. A more detailed description of the BOS technique can be found in Raffel (2015).

2.4 Overview of the performed wind tunnel runs

In order to study the evolution of the shock features and of the buffet frequency with the aerodynamic conditions, runs with constant M_∞ and AOA are performed. The angle of attack is varied between 5° and 6.5° with a spacing of 0.5°, whereas the Mach number is changed between 0.72 and 0.75 in steps of 0.01. These combinations of aerodynamic parameters are chosen to be either developed buffet or incipient buffet flows. The analyzed AOAs are relatively higher than those in Jacquin et al (2009), Crouch et al (2009b), Deck (2005) and Thiery and Coustols (2005) due to a buffet onset delay. As explained in Accorinti et al (2022), this delay may be caused by the wall suction excessively reducing the local Mach number on the wing in the presence of shock waves. However, a correction for the effective AOA and M_∞ is not available. The sampling frequency of the image recording is 1 kHz and the number of samples per run is 10,000. The stagnation conditions are set to $p_0 \approx 1.5 \times 10^5$Pa and $T_0 \approx 300$K, in order to yield a Reynolds number based on the chord equal to $Re_c \approx 3 \times 10^6$, as in Jacquin et al (2009).

2.5 Shock detection

The BOS displacement field is obtained via cross-correlation between the wind-off and the wind-on images, by setting the interrogation area to 8 pixels (2 mm) with an overlap of 50%. Then, it undergoes the following post-processing to facilitate shock detection. First, a median filter is applied to each point of the displacement field to reduce the noise in the signal. This filter is centered on the considered point and large 12x12 pixels. The median filter slightly alters the shock gradient value but does not affect the detected shock location. Afterward, the gradient of the BOS displacement field in the streamwise direction is computed, which is proportional to the gradient of the density gradient. By doing
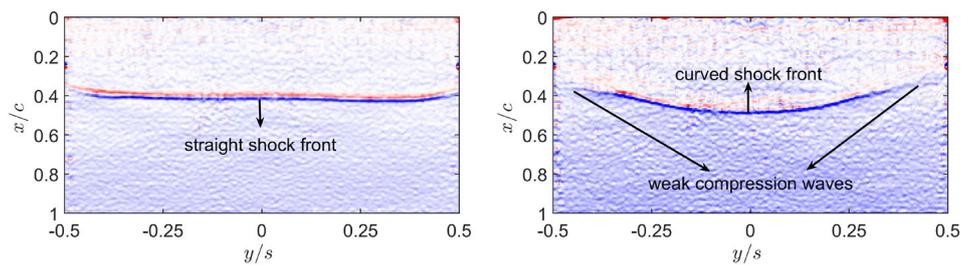
Fig. 3 Color-coded gradient of the BOS displacement field for $M_\infty = 0.74$ at two different angles of attack: straight shock front with small side-wall effects at AOA = 6.5° (left), and curved shock front with stronger side-wall effects and weaker shock at the wing ends at AOA = 5° (right)

so, it is possible to remove the signal peaks linked to residual noise or the model's vibration, and solely focus on the density gradient associated with the shock.

An example of BOS displacement gradient is illustrated in Fig. 3 left for $M_\infty = 0.74$ and AOA = 6.5° at one time instant. The red and blue curves represent, respectively, an increase and a decrease in the positive density gradient introduced by the shock wave. The shock location can be easily identified with the zero value (white) straddling the two curves. In fact, the zero of the signal's gradient highlights the location where the maximum density gradient is reached. This snapshot is representative of the flow features at higher Mach numbers and angles of attack, whereby the shock front appears straight and easily detectable by using the criterion described above. Solely very close to the span ends, the blue and red lines tend to fade, sign that there is no strong density gradient there. As explained in Jacquin et al (2009), this is caused by the interaction of the shock with the side-wall boundary layer. For these spanwise positions, no reliable shock detection can be retrieved.

At lower Mach numbers and/or angles of attack, the side-wall boundary layer effects are expected to be stronger and to involve a larger portion of the wing. An example of this is shown in Fig. 3 right, where the gradient of the BOS displacement field is illustrated for $M_\infty = 0.74$ and AOA = 5° at one time instant. In this case, the red and the blue lines are not clearly visible for 10-15% of the span at each span end. There, weak compression waves are present instead of a clear shock wave. Moreover, the shock front looks significantly more curved.

In order to investigate how significant the spanwise variation of the shock front features are a single-time snapshot does not suffice. For this reason, all the 10,000 samples of each run are employed to perform a statistical and frequency analysis of the shock front.

In the electronic supplementary material available online, the videos of the first 100 time instants of the BOS displacement gradient are uploaded for $M_\infty = 0.74$ and all the investigated AOAs.

3 Results

This section is divided into three parts. In the first one, the statistics (time average and standard deviation) of the reliably detected spanwise shock locations are plotted together with the standard deviation of the BOS displacement gradient for several AOAs and $M_\infty = 0.74$. Furthermore, the time averages of the shock at three spanwise locations ($y/s = -0.40$, $y/s = 0$ and $y/s = 0.40$) are shown for all the Mach numbers in Table 1 in correspondence of the column "$\overline{x_s/c}$ at y/s". For the aerodynamic cases where no clear shock is detected at $y/s = -0.40$ and $y/s = 0.40$ due to the side-wall effects, the maximum along the chord of the standard deviation of the BOS displacement gradient is selected instead. This provides an estimation of the time-averaged location of the weaker compression waves at the wing ends.

The standard deviations of the shock at the three spanwise locations are given too for all the Mach numbers in Table 1, at the column marked by the symbol "$\sigma_{x_s/c}$ at y/s". For the aerodynamic cases where no shock is detected at $y/s = -0.40$ and $y/s = 0.40$, only the value corresponding to $y/s = 0$ is given.

For the sake of completeness and comparison, the time average and the standard deviation of the shock measured for the same aerodynamic conditions in Accorinti et al (2022) are shown in Table 1, in correspondence of the columns "$\overline{x_s/c}$ at ζ/c" and "$\sigma_{x_s/c}$ at ζ/c", respectively. These statistics, which were obtained via BOS measurements from the side, are presented for two different normal distances from the upper surface, namely at $\zeta/c = 0.10$ and $\zeta/c = 0.30$.

In the second part of the section, the PSD of the oscillations of the reliably detected spanwise shock locations is plotted for several AOAs and $M_\infty = 0.74$. However, the measured buffet frequencies and reduced frequencies for all the four Mach numbers are collected in Table 1 in correspondence of the columns f_{buffet} and k_{buffet}, respectively. Since the buffet frequency turns out to be constant along the span, the values are not shown for each of the three analyzed span positions, as done for $\overline{x_s/c}$. The frequencies found in

Accorinti et al (2022) are not shown in separate columns since they are identical to the ones measured via BOS from the top.

In the last part, the correlation of the reliably detected shock locations with the one at $y/s = 0$ is plotted for several AOAs and $M_\infty = 0.74$.

All the plots for $M_\infty = 0.72$, $M_\infty = 0.73$, and $M_\infty = 0.75$ are omitted since they are qualitatively similar to the ones presented for $M_\infty = 0.74$.

Moving farther away from the mid-span portion sharpens the differences with respect to the shock location at $y/s = 0$. In fact, unsteady weaker compression waves are present instead of a clear shock wave. At $y/s = \pm0.40$, for instance, the time-averaged location of these waves is $5 - 6\%$ of the chord upstream of the shock at $y/s = 0$. Furthermore, the compression waves seem to oscillate within 10% of the chord. This is indeed the chordwise width of the region with a significant standard deviation of the BOS displacement gradient in Fig. 4. The higher chordwise amplitude of fluc-

Fig. 4 Color-coded standard deviation of BOS displacement gradient, time-averaged shock location (black curve) and standard deviation of shock location (black error bar) for $M_\infty = 0.74$
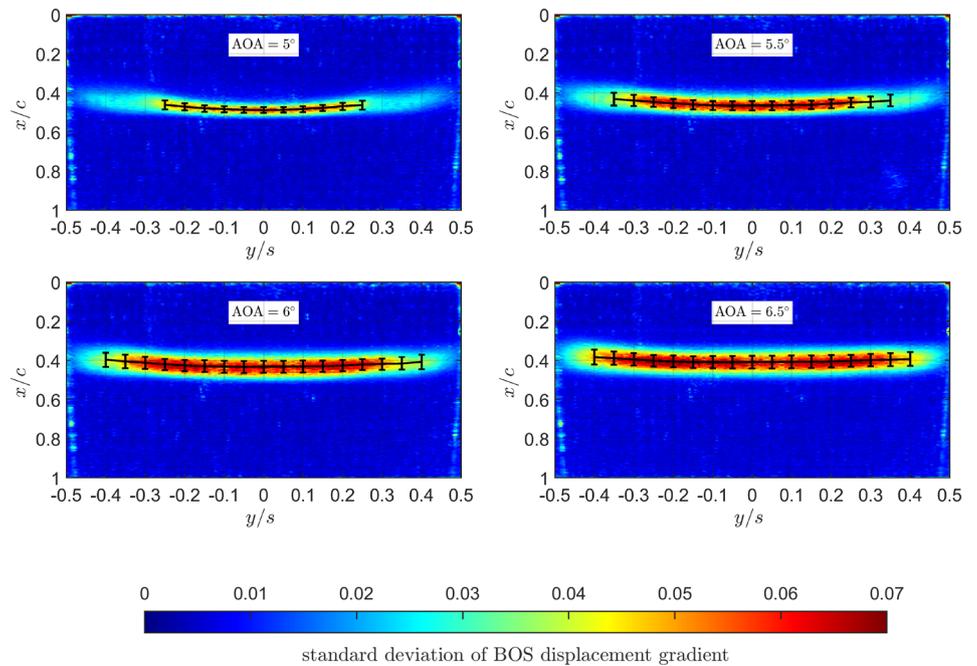
3.1 Shock front statistics

In Fig. 4, the standard deviation of the BOS displacement gradient field is shown for several AOAs and $M_\infty = 0.74$. The time averages (black curve) and the standard deviations (black error bar) of the detected shock front are also plotted, but only for the spanwise locations where the detection algorithm reliably works. In fact, as already explained in Sect. 2.5, getting closer to the wing ends, the density gradient in the shock region significantly weakens and does not always show a clear maximum. This leads to falsely detected shock positions at several time instants, which in turn would alter the shock statistics.

At AOA $= 5°$, the shock can be clearly detected for $-0.25 < y/s < 0.25$. The shock front in the mid-span region appears relatively straight, with the shock location at $y/s = \pm0.25$ being only 2.5% of chord displaced upstream relative to the one at $y/s = 0$. The standard deviation of the shock oscillations progressively increases from 0.015, at $y/s = 0$, to 0.023, at $y/s = \pm0.25$.

tuations at the wing ends is due to the interaction with the side-wall boundary layer on the side walls, and not to buffet. This is supported by the fact that the amplitude of fluctuations is very low in the mid-span region and monotonically soars toward the wing ends.

As can be seen in Table 1, the time-averaged shock location measured via BOS from the side in Accorinti et al (2022) at $\zeta/c = 0.10$ is slightly more upstream than the one in the mid-span portion captured from the top. Since the latter is the strongest shock along the span, one would expect to see the very same shock also from the side. The fact that this is not the case is likely due to the spanwise curvature of the shock front. Since the shock location seen from the side is the result of integration along the wing span, and considering that the shock position is swiftly changing from the center of the span toward its ends (see again Fig. 4), it is reasonable to expect an integrated shock location from the side approximately between the mid-span and the wing-end ones observed from the top. The standard deviation of the shock location

Table 1 Summary of results

AOA [°]	M_∞	$\overline{x_s/c}$ at y/s −0.40, 0, 0.40	$\sigma_{x_s/c}$ at y/s −0.40, 0, 0.40	$\overline{x_s/c}$ at ζ/c 0.10, 0.30	$\sigma_{x_s/c}$ at ζ/c 0.10, 0.30	f_{buffet} [Hz]	k_{buffet}
5.1	0.72	0.37, 0.42, 0.38	0.014	0.40, 0.41	0.019, 0.018		
5.6	0.72	0.38, 0.43, 0.37	0.014	0.41, 0.43	0.022, 0.017		
6	0.72	0.36, 0.42, 0.39	0.020	0.39, 0.42	0.033, 0.020	90	0.177
6.5	0.72	0.36, 0.39, 0.37	0.033	0.36, 0.40	0.033, 0.026	105	0.208
5.0	0.73	0.40, 0.45, 0.40	0.015	0.43, 0.44	0.018, 0.019		
5.5	0.73	0.41, 0.46, 0.40	0.015	0.43, 0.45	0.019, 0.019		
6	0.73	0.39, 0.43, 0.40	0.029	0.40, 0.43	0.030, 0.025	98	0.193
6.5	0.73	0.38, 0.40, 0.38	0.039, 0.034, 0.037	0.37, 0.40	0.032, 0.027	111	0.223
5.0	0.74	0.44, 0.49, 0.43	0.015	0.47, 0.48	0.018, 0.016		
5.5	0.74	0.43, 0.47, 0.43	0.024	0.44, 0.46	0.026, 0.023	95	0.188
6	0.74	0.40, 0.43, 0.41	0.036, 0.030, 0.037	0.40, 0.44	0.038, 0.026	104	0.208
6.5	0.74	0.38, 0.41, 0.39	0.038, 0.031, 0.034	0.38, 0.41	0.030, 0.027	117	0.233
4.9	0.75	0.46, 0.49, 0.47	0.020	0.47, 0.49	0.021, 0.019	94	0.182
5.5	0.75	0.44, 0.47, 0.43	0.024	0.44, 0.47	0.025, 0.022	104	0.208
5.9	0.75	0.42, 0.44, 0.42	0.038, 0.028, 0.033	0.41, 0.45	0.034, 0.025	111	0.223
6.4	0.75	0.40, 0.42, 0.41	0.039, 0.031, 0.034	0.39, 0.43	0.038, 0.027	120	0.238

detected from the side is also slightly higher than the one of the shock at $y/s = 0$ seen from the top. This is probably due to the fact the shock location detected from the side occasionally jumps between one span position and another, which in turn introduces an additional fictive streamwise oscillation.

At AOA = 5.5°, the shock can be clearly detected for $−0.35 < y/s < 0.35$. The level of shock oscillations is significantly higher and more homogeneously distributed over the span, which remarks the stronger two-dimensionality of the flow. In fact, the entire shock front appears straighter. Also, at $y/s = ±0.40$, the time-averaged location of the compression waves is now only 4% of the chord upstream of the shock location at $y/s = 0$. Increasing the angle of attack has shifted the shock location in the middle of the span upstream. This phenomenon, the so-called inversion of the shock motion, is a sign of boundary layer separation behind the shock and was recently proved by Accorinti et al (2022) to be a necessary condition for buffet onset. Another compelling aspect is that, on the other hand, the compression wave locations at the wing ends have hardly moved. A possible reason for this could be that the shock close to the span ends is not strong enough to cause a separation of the boundary layer and, consequently, an inversion of the shock motion.

At AOA = 6°, the shock can be clearly detected for $−0.40 < y/s < 0.40$. The level of shock oscillations has again soared. The entire shock front appears to have moved upstream and to be straighter at the wing ends, the time-averaged shock location is now located $2 − 3$% of the chord upstream of the one at $y/s = 0$. The inversion of shock

motion is now evident also for the shock positions at the wing ends.

Even though the spanwise shape of the shock front has become straighter, the difference between the time averages of the shock location detected from the side at $\zeta/c = 0.10$ and from the top at $y/s = 0$ does not diminish (see Table 1). A possible explanation for this could be the following. Once separation occurs, the shock wave displays the characteristic lambda shape at its foot. This implies that, observed from the side, the vertical shape of the shock front appears oblique close to the surface, with the streamwise shock position rapidly shifting downstream while moving up along the fore shock leg. On the other hand, above the triple point, the streamwise shock location stays approximately constant (normal shock). The normal shock is generally less strong than the fore shock leg. Therefore, one would expect that the maximum density gradient visualized from the top corresponds to the fore shock leg. However, the shock location detected from the top is the result of integrating along the vertical distance. The streamwise normal-shock location is integrated for a much longer vertical distance than the single fore-shock-leg locations, which change along z. So, whereas the BOS-from-the-side streamwise shock location at $\zeta/c = 0.10$ corresponds to the fore shock leg, the BOS-from-the-top streamwise shock location possibly reflects more the normal shock above the triple point.

If this assumption were correct, selecting the streamwise location of the normal shock detected from the side should significantly improve the agreement with the BOS-from-the-top results. $\zeta/c = 0.30$ is chosen since, above it, the shock appeared normal in Accorinti et al (2022) for all the investigated cases. The respective time-averages and

standard deviations are shown in Table 1. The agreement with the streamwise shock location at $y/s = 0$ is now excellent. Increasing the angle of attack enlarges the flow separation extent and, at the same time, the inclination and vertical extent of the fore shock leg. Therefore, it enhances the difference between the streamwise shock location detected from the side at $\zeta/c = 0.10$ and the one detected from the top at $y/s = 0$. On the other hand, the streamwise location of the normal shock ($\zeta/c = 0.30$) always maintains a superb agreement with the mid-span shock location.

At AOA = 6.5°, the shock can be clearly detected for $-0.40 < y/s < 0.40$. The level of shock oscillations only slightly increases.

3.2 Frequency content of the spanwise shock locations

The PSD of the reliably detected shock front fluctuations is analyzed to determine its dominant frequencies, with a particular focus on the spanwise frequency distribution. The PSD is computed between 1 and 500 Hz with a resolution of 1 Hz, using the method of Welch presented in Welch (1967). A window width of 100-time steps is selected to have a sufficient number (approximately 10) of buffet cycles in it.

In Fig. 5, the color-coded PSD of the shock oscillations is illustrated in a logarithmic scale for several AOAs and $M_\infty = 0.74$. At AOA = 5°, the level of shock fluctuations

in the central region ($-0.10 < y/s < 0.10$) is relatively low, as already seen in Fig. 4. Moreover, there is a clear gap between low frequencies ($f < 50$ Hz) and $f = 85$ Hz. As already described in Accorinti et al (2022), buffet onset is detected at AOA = 4.9° for this Mach number. Therefore, the slight peak found in the present work at 85 Hz corresponds to an incipient buffet.

Moving toward the wing ends, the PSD amplitudes increase by one order of magnitude. This is in line with the large oscillations of the weak compression waves shown in Fig. 4 in the proximity of the span ends. Due to the absence of a clearly established shock wave, the buffet frequency measured in the middle of the span can not be easily distinguished in this portion of the span. The low frequencies become more and more dominant; in particular, high contributions to the shock oscillations can be seen up to 50 Hz, moving from $y/s = \pm0.10$ to $y/s = \pm0.25$. In Jacquin et al (2009) and Sugioka et al (2022), it was shown via oil flow visualizations that the shock at the span ends is affected by the side-wall boundary layer. Based on this, the hypothesis may be advanced that the low-frequency broadband component ($1 < f < 50$ Hz, $0 < St < 0.031$) observed in the shock spectrum derives from the interaction of the shock with the side-wall boundary layer. However, the application of another technique (for instance PIV) that resolves the flow field and its frequency content at the span ends is needed to confirm this assumption.

Fig. 5 Color-coded PSD of shock oscillations for several AOAs and $M_\infty = 0.74$
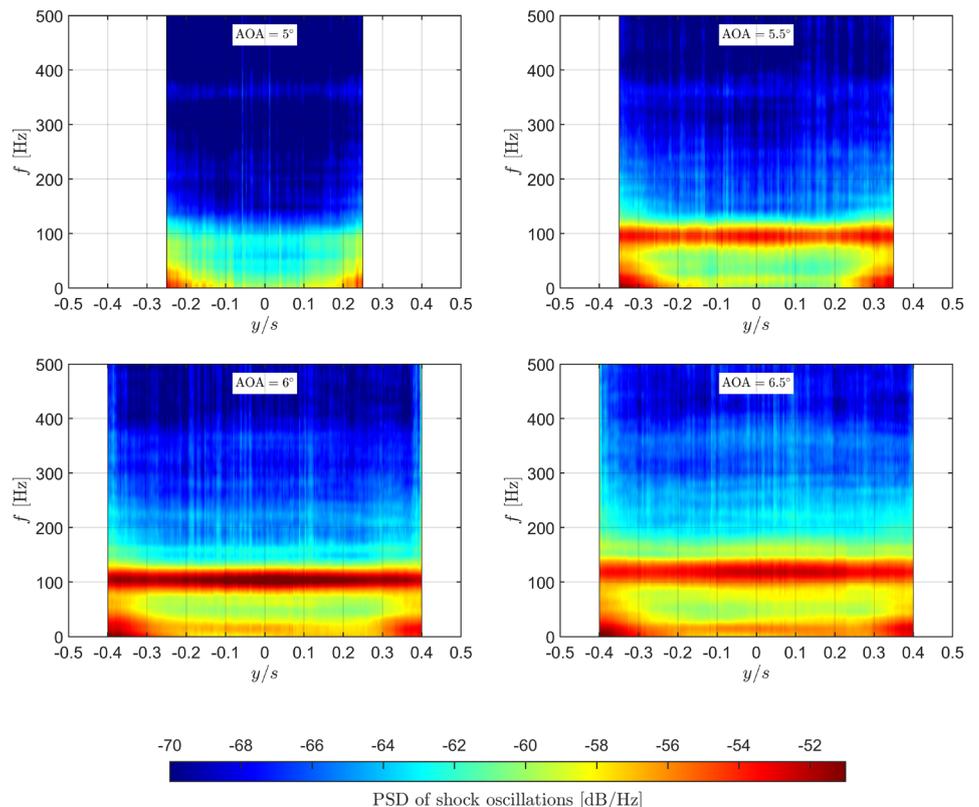
At AOA = 5.5°, the intensity of the PSD amplitude in the central region has increased by almost an order of magnitude and is now rather uniform between $y/s = 0$ and $y/s = \pm 0.20$. A clear peak centered at $f = 95$ Hz can be observed, which suggests a developed buffet is present. This is confirmed by the findings in Accorinti et al (2022). Starting from $y/s = \pm 0.20$, the contributions of low frequencies soar, until becoming dominant at $y/s = \pm 0.30$. Moving farther toward the wing ends, it looks like the buffet and the low-frequency broadband merge, leading to a large region of high PSD amplitudes between 1 and 100 Hz.

At AOA = 6°, the intensity of the PSD amplitude of the buffet frequency, which lies now at $f = 104$ Hz, has further increased by almost an order of magnitude. Moreover, it is clearly dominant over the entire plotted spanwise range $(-0.40 < y/s < 0.40)$. Contributions from very low frequencies ($1 < f < 25$ Hz, $0 < St < 0.016$) with a maximum at 14 Hz are now visible also in the central part of the wing. Moving from $y/s = 0$ to $y/s = \pm 0.25$, the bandwidth of the low frequencies stays constant. Only starting from $y/s = \pm 0.25$ shifts the upper limit of the low frequencies toward the buffet frequency, leading to the low-frequency broadband ($1 < f < 50$ Hz) already seen at AOA = 5° and AOA = 5.5°. This suggests that the low-frequency content in the middle of the span may be different from the low-frequency broadband developing toward the span ends.

The origin of the mid-span low-frequency content is not clear. In Jacquin et al (2009), no sign of low frequencies is visible in the PSD of the pressure signal in the mid-span region and $x/c = 0.60$. In the PSD of the shock oscillation at $y/s = 0$ reported by D'Aguanno et al (2021), there is no trace of these low frequencies either. The oil visualizations performed by Jacquin et al (2009) revealed the presence of steady vortices in the shock-induced separated boundary layer at the mid-span region. Based on these findings, we advance the hypothesis that the interaction of these vortices with the shock may be the cause of the low-frequency content in the middle of the span. On the other hand, unsteady separated boundary layers typically exhibit higher frequency contents.

For this reason, the application of another technique (for instance PIV) that resolves the velocity field in the mid-span region is necessary to ascertain whether the steady vortices reported in Jacquin et al (2009) are present here too and display high fluctuations at low frequencies. The PSD of the heave motion measured in Accorinti et al (2022) shows a small peak at 30 Hz. This peak is present at lower angles of attack too, where the shock spectrum does not display the low-frequency content in the mid-span region. This and the fact that the heave peak is not at 14 Hz speak for the heave motion not being responsible for the low-frequency content characterizing the developed buffet cases. However, further investigation is required to completely rule out structural vibrations as a possible cause of the low-frequency content seen in the shock spectrum.

Finally, a new frequency with rather low amplitudes can be seen at 157 Hz between $y/s = 0$ and $y/s = \pm 0.30$. As already reported in Accorinti et al (2022), this is linked to the heave structural mode, which is activated once buffet develops. Since the two frequencies are remarkably close to each other, an FSI is facilitated. However, it should be noted that the heave peak is more than one order of magnitude lower than the buffet one.

At AOA = 6.5°, the intensity of the PSD amplitude of the buffet frequency has decreased. A narrow sharp peak is solely present between $y/s = -0.10$ and $y/s = 0.20$. Moreover, the buffet frequency has shifted to 118 Hz. Also, the bandwidth of buffet frequency has considerably enlarged. As already reported in Accorinti et al (2022), this is probably due to an intensified interaction with the heave mode, which leads to the formation of a broader peak. In addition, there seems to be an interaction between the low frequencies ($1 < f < 25$ Hz) in the middle of the span and the buffet one. In fact, the lower limit of the buffet bandwidth appears to move to lower frequencies. The presence of the low-frequency broadband ($1 < f < 50$ Hz) is limited to the spanwise ends; in particular, its amplitude is comparable to the buffet one only at $y/s = \pm 0.40$. Finally, higher frequencies ($200 < f < 350$ Hz) appear in the spectrum, albeit with low amplitudes.

3.3 Correlation of shock locations

In Fig. 5, it was shown how, once shock buffet settles (AOA = 5.5°), its frequency is dominant and constant along the span. However, the PSD of the shock oscillations does not reveal any information regarding the phase, if present, between two different spanwise shock locations. With this objective, the correlation of shock locations, $R_{x_s x_s}$, is computed at various spanwise positions on the model's upper surface. $R_{x_s x_s}$ is defined as follows:

$$R_{x_s x_s}(n, m, \tau) = \frac{\overline{x'_{s_n}(t) x'_{s_m}(t + \tau)}}{\sqrt{\overline{x'_{s_n}(t)^2}} \sqrt{\overline{x'_{s_m}(t)^2}}}, \qquad (1)$$

where $x'_{s_n}(t)$ and $x'_{s_m}(t + \tau)$ represent the fluctuations of the shock locations at the spanwise positions y_n and y_m respectively, the second data set having been shifted by τ. Their product is then averaged over all time steps, t. As for $\sqrt{\overline{x'_{s_n}(t)^2}}$ and $\sqrt{\overline{x'_{s_m}(t)^2}}$, they represent the standard deviation of both fluctuating shock locations. The reference shock position is selected at the span's center ($y_n/s = 0$), whereas y_m is swept within the portion of the span where the shock

Fig. 6 Color-coded correlation of the shock locations with the one at $y/s = 0$ for several AOAs and $M_\infty = 0.74$
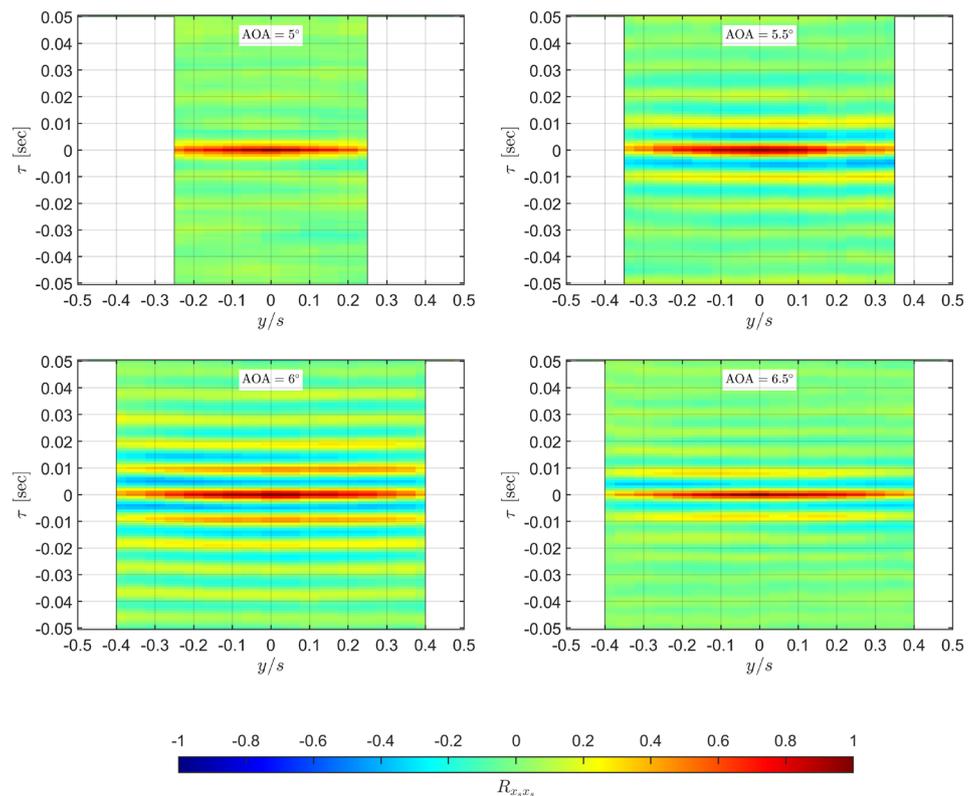
detection was successful and not impeded by the interaction of the shock with the side-wall boundary layer (see Fig. 4).

In Fig. 6, the color-coded correlation of the shock locations with the one at $y/s = 0$ is illustrated for $M_\infty = 0.74$.

At AOA = 5°, for which the analyzed shock locations are $-0.25 \leq y_m/s \leq 0.25$, high correlation values can be seen only for $\tau = 0$, which suggests that there is no strong periodicity in the flow. This is in line with Fig. 5, where no dominant frequency is visible for this angle of attack.

At AOA = 5.5°, for which the considered shock locations are $-0.35 \leq y_m/s \leq 0.35$, a periodic pattern appears in the figure. Red and blue "stripes" indicate high positive and negative correlation values, respectively. For each stripe, the correlation peaks are detected, which are reached at the same time along the entire analyzed span. This implies that the shock front oscillates without appreciable phases between different spanwise shock locations. The time shift between two consecutive positive or negative correlation peaks is ≈ 0.011 sec, which corresponds to the buffet frequency of 95 Hz found in Fig. 5.

However, it should be noted that between $-0.35 \leq y_m/s \leq -0.25$ and $0.25 \leq y_m/s \leq 0.35$ the correlation values drop. In these regions, as shown in Fig. 5, the shock oscillation is also characterized by a lower frequency introduced by the interaction with the side-wall boundary layer at the wing ends. This is the reason why the correlation

with the shock oscillation at $y/s = 0$, which is mostly regulated by buffet, weakens.

At AOA = 6°, for which the analyzed shock locations are $-0.40 \leq y_m/s \leq 0.40$, the periodic pattern becomes more evident, that is the correlation values soar everywhere and the periodicity can be observed for several buffet cycles. The time shift between two red (or blue) stripes is ≈ 0.010 sec, which corresponds to the buffet frequency of 104 Hz found in Fig. 5. For this angle of attack too, no phase delay can be detected along the span. Moreover, the correlation peaks maintain high values across the entire considered span. This is due to the fact that, as visible in Fig. 5, the buffet frequency is dominant everywhere. Only starting from $y/s = -0.40$ does the PSD intensity associated with the broad-banded low-frequency contributions become comparable with the buffet one.

At AOA = 6.5°, the periodic pattern begins to fade away, which is in line with the results illustrated in Fig. 5, where the PSD amplitude of buffet frequency diminishes with respect to the one at AOA = 6°. This can be traced back either to buffet offset and/or to the interaction with the heave structural mode. The time shift between two red (or blue) stripes is ≈ 0.008 sec, which corresponds to the buffet frequency of 118 Hz found in Fig. 5.

4 Summary and conclusions

The focus of the present work was to provide the shock front dynamics on a 2-D wing for several combinations of aerodynamic parameters (angle of attack and Mach number). For this reason, a supercritical profile (OAT15A) with aspect ratio 2 was experimentally investigated at the Trisonic wind tunnel Munich by means of BOS measurements. This technique allowed for examining the span variation of the shock front statistics and frequency content. The main results of the present work, which reflect the goals described in Sect. 1.4, can be summarized as follows:

– The side-wall boundary layer has two main effects on the spanwise distribution of the shock statistics. First, moving away from the mid-span region, the side-wall boundary layer weakens the shock and shifts upstream its location. In the proximity of the side walls, weak compression waves are visible instead of a clear shock. At incipient buffet conditions, the portion of the shock front that is strongly affected by the side-wall boundary layer seems larger than in Jacquin et al (2009) and Sugioka et al (2022) (25% vs 10% and 15%, respectively). This can be traced back to the much smaller aspect ratio (2 vs 3.4 and 4.5). However, the side-wall boundary layer effects decrease with an increase in the angle of attack or Mach number. In fact, once buffet establishes, the time-averaged shock front remarkably curves and weakens only starting from 10% of distance from each span end, just like in Jacquin et al (2009) and Sugioka et al (2022). Therefore, one may argue that buffet onset smooths out the differences in boundary effects introduced by different aspect ratios. Second, the chordwise amplitude of the flow fluctuations soars moving from the mid-span region to the span ends. This is due to the fact that the weak compression waves at the wing ends are more sensitive than an established shock to the unsteady side-wall boundary layer. However, once buffet establishes, the amplitude of shock oscillations becomes homogeneous for most of the span. Only in the last 10% of the span at each wing end can slightly higher fluctuations be detected.

– The power spectral density of the shock oscillations shows four main contributions. The first one encompasses low frequencies up to 50 Hz. This low-frequency broadband can be observed in both pre-buffet and buffet flows at the span ends. The hypothesis was advanced that it is linked to the side-wall boundary layer, which exists independently from shock buffet, as reported by Jacquin et al (2009) and Sugioka et al (2022). However, the application of another technique that resolves the flow field and its frequency content at the span ends is

needed to confirm this assumption. The second contribution stems out of low frequencies up to 25 Hz and appears in the central part of the span only after buffet onset. Even though the model vibration does not show a similar frequency content, further investigation is needed to completely rule out its involvement. The hypothesis was stated that the interaction of the shock with the vortices that were detected in the mid-span separated area in Jacquin et al (2009) and Sugioka et al (2022) is responsible for the low-frequency content. The application of another technique could resolve the shock-induced separated boundary layer in the mid-span portion. This way, it would be possible to verify whether the vortices reported in the literature are actually present and responsible for the low-frequency contents of the shock oscillation in the mid-span region. The third contribution is the buffet frequency. Initially, at incipient buffet, it appears only in the mid-span area. After buffet has been established, it is homogeneously present along the entire span. Furthermore, it is by far the most dominant frequency of shock oscillations. Only in the last 15-10% of the span at each wing's end becomes the PSD amplitude of the low-frequency broadband comparable. The final contribution originates from the heave structural mode and becomes evident only after buffet onset. However, it should be noted that its amplitude is almost one order of magnitude smaller than the amplitude of all the other above-mentioned frequencies.

The fluid and structural modes associated with the above-mentioned frequencies appear to interact with each other. At the span ends, there seems to be an interaction between the buffet mode and the side-wall broad-banded mode so that also the frequencies between 50 Hz and the buffet frequency show significant contributions. In the mid-span region, the buffet mode interacts with the low frequencies, which leads to a broader buffet peak. Moreover, there is also an interaction between the heave structural and the fluid modes, which is facilitated by the fact that they have very similar frequencies.

– The shock locations in the central part of the wing span display high correlation values with the shock at $y/s = 0$. The span portion with high correlation extends toward the span ends after buffet onset. No phase delay between shocks at different span positions is measured.

Based on these observations, it can be concluded that the self-sustained shock oscillations in the present study are the result of the superposition of several modes. Those possibly linked to the side-wall boundary layer and to the steady vortices in the middle of the span cause a spanwise variation of the shock oscillation spectrum. However, the shock oscillations display a remarked 2-D behavior. This

is due to the well-known 2-D buffet, which appears to be the dominant fluid mode in the flow.

Author Contributions Alessandro Accorinti wrote the manuscript. All the other authors contributed by providing insightful suggestions and revising the manuscript.

Availability of data and materials Not applicable.

Declarations

Ethical Approval Not applicable.

Conflict of interest Not applicable.

References

Accorinti A, Baur T, Scharnowski S, Kähler CJ (2022) Experimental investigation of transonic shock buffet on an OAT15A profile. AIAA J Adv Online Publ 60(11):6289–6300. https://doi.org/10.2514/1.J061135

Brion V, Dandois J, Abart JC, Paillart P (2017) Experimental analysis of the shock dynamics on a transonic laminar airfoil. Progress Flight Phys 9:365–386. https://doi.org/10.1051/eucass/201690365

Crouch JD, Garbaruk A, Magidov D, Jacquin L (2009a) Global structure of buffeting flow on transonic airfoils. In: IUTAM symposium on unsteady separated flows and their control. Springer, pp 297–306. https://doi.org/10.1007/978-1-4020-9898-7_25

Crouch JD, Garbaruk A, Magidov D, Travin A (2009) Origin of transonic buffet on aerofoils. J Fluid Mech 628:357–369. https://doi.org/10.1017/S0022112009006673

D'Aguanno A, Schrijer F, van Oudheusden B (2021) Spanwise organization of upstream traveling waves in transonic buffet. Physics of Fluids 33(10):106105. https://doi.org/10.1063/5.0062729

Deck S (2005) Numerical simulation of transonic buffet over a supercritical airfoil. AIAA J 43(7):1556–1566. https://doi.org/10.2514/1.9885

D'Aguanno A, Schrijer FFJ, van Oudheusden BW (2021) Experimental investigation of the transonic buffet cycle on a supercritical airfoil. Exp Fluids 62(10):1–23. https://doi.org/10.1007/s00348-021-03319-z

Garnier E, Deck S (2010) Large-eddy simulation of transonic buffet over a supercritical airfoil. In: Turbulence and Interactions: Proceedings the TI 2009 Conference. Springer, pp 135–141. https://doi.org/10.1007/978-3-642-14139-3_16

Giannelis NF, Levinski O, Vio GA (2018) Influence of mach number and angle of attack on the two-dimensional transonic buffet phenomenon. Aerosp Sci Technol 78:89–101. https://doi.org/10.1016/j.ast.2018.03.045

Hartmann A, Feldhusen A, Schröder W (2013) On the interaction of shock waves and sound waves in transonic buffet flow. Phys Fluids 25(2): https://doi.org/10.1063/1.4791603

Iovnovich M, Raveh DE (2012) Reynolds-averaged Navier–Stokes study of the shock-buffet instability mechanism. AIAA J 50(4):880–890. https://doi.org/10.2514/1.J051329

Iovnovich M, Raveh DE (2015) Numerical study of shock buffet on three-dimensional wings. AIAA J 53(2):449–463. https://doi.org/10.2514/1.J053201

Jacquin L, Molton P, Deck S, Maury B, Soulevant D (2009) Experimental study of shock oscillation over a transonic supercritical profile. AIAA J 47(9):1985–1994. https://doi.org/10.2514/1.30190

Kokmanian K, Scharnowski S, Schäfer C, Accorinti A, Baur T, Kähler CJ (2022) Investigating the flow field dynamics of transonic shock buffet using particle image velocimetry. Exp Fluids 63(9):1–14. https://doi.org/10.1007/s00348-022-03499-2

Korthäuer T, Accorinti A, Scharnowski S, Kähler CJ (2022) The effect of Mach number and pitching eigenfrequency on transonic buffet onset. AIAA J Adv Online Publ. https://doi.org/10.2514/1.J061915

Lee BHK (1990) Oscillatory shock motion caused by transonic shock boundary-layer interaction. AIAA J 28(5):942–944. https://doi.org/10.2514/3.25144

Lee BHK (2001) Self-sustained shock oscillations on airfoils at transonic speeds. Prog Aerosp Sci 37(2):147–196. https://doi.org/10.1016/S0376-0421(01)00003-3

McDevitt JB, Okuno AF (1985) Static and dynamic pressure measurements on a NACA 0012 airfoil in the Ames high Reynolds number facility, vol 2485. National Aeronautics and Space Administration, Scientific and Technical Information Branch. https://ntrs.nasa.gov/api/citations/19850019511

Nitzsche J (2009) A numerical study on aerodynamic resonance in transonic separated flow. In: IFASD 2009, international forum on aeroelasticity and structural dynamics, Seattle, WA (USA), pp 1–18. https://elib.dlr.de/61964/

Nitzsche J, Ringel LM, Kaiser C, Hennings H (2019) Fluid-mode flutter in plane transonic flows. https://elib.dlr.de/127989/

Pearcey HH (1958) A method for the prediction of the onset of buffeting and other separation effects from wind tunnel tests on rigid models. Tech. Rep. 223, Advisory Group for Aerospace Research and Development

Raffel M (2015) Background-oriented schlieren (bos) techniques. Exp Fluids 56(3):1–17. https://doi.org/10.1007/s00348-015-1927-5

Raghunathan S, Mitchell R, Gillan M (1998) Transonic shock oscillations on naca0012 aerofoil. Shock Waves 8(4):191–202. https://doi.org/10.1007/s001930050113

Sartor F, Mettot C, Sipp D (2015) Stability, receptivity, and sensitivity analyses of buffeting transonic flow over a profile. AIAA J 53(7):1980–1993. https://doi.org/10.2514/1.J053588

Scharnowski S, Bross M, Kähler CJ (2019) Accurate turbulence level estimations using piv/ptv. Exp Fluids 60(1):1–12. https://doi.org/10.1007/s00348-018-2646-5

Scheitle H, Wagner S (1991) Influences of wind tunnel parameters on airfoil characteristics at high subsonic speeds. Exp Fluids 12(1):90–96. https://doi.org/10.1007/BF00226571

Schlichting H, Gersten K (2017) Boundary-layer theory. Springer, Berlin. https://doi.org/10.1007/978-3-662-52919-5

Sugioka Y, Kouchi T, Koike S (2022) Experimental comparison of shock buffet on unswept and 10-deg swept wings. Exp Fluids 63(8):1–18. https://doi.org/10.1007/s00348-022-03482-x

Thiery M, Coustols E (2005) Urans computations of shock-induced oscillations over 2d rigid airfoils: influence of test section geometry. Flow Turbul Combust 74(4):331–354. https://doi.org/10.1007/s10494-005-0557-z

Welch PD (1967) The use of fast fourier transform for the estimation of power spectra: A method based on time averaging over short, modified periodograms. IEEE Trans Audio Electroacoust 15(2):70–73. https://doi.org/10.1109/TAU.1967.1161901

Xiao Q, Tsai HM, Liu F (2006) Numerical study of transonic buffet on a supercritical airfoil. AIAA J 44(3):620–628. https://doi.org/10.2514/1.16658